ARMY RESEARCH LABORATORY

Validation of the U.S. Army Research Laboratory's Gun Dynamics Simulation Codes for Prototype Kinetic Energy

by James F. Newill, Bernard J. Guidos, and Carl D. Livecchia

ARL-TR-3039 September 2003

NOTICES

Disclaimers

The findings in this report are not to be construed as an official Department of the Army position unless so designated by other authorized documents.

Citation of manufacturer's or trade names does not constitute an official endorsement or approval of the use thereof.

Destroy this report when it is no longer needed. Do not return it to the originator.

Army Research Laboratory
Aberdeen Proving Ground, MD 21005-5066

ARL-TR-3039 **September 2003**

Validation of the U.S. Army Research Laboratory's Gun Dynamics Simulation Codes for Prototype Kinetic Energy

James F. Newill and Bernard J. Guidos
Weapons and Materials Research Directorate, ARL

Carl D. Livecchia
U.S. Army Research, Development, and Engineering Center

REPORT DOCUMENTATION PAGE

Form Approved
OMB No. 0704-0188

1. REPORT DATE *(DD-MM-YYYY)*	2. REPORT TYPE	3. DATES COVERED (From - To)
September 2003	Final	September 1995–September 2002

4. TITLE AND SUBTITLE
Validation of the U.S. Army Research Laboratory's Gun Dynamics Simulation Codes for Prototype Kinetic Energy

5a. CONTRACT NUMBER

5b. GRANT NUMBER

5c. PROGRAM ELEMENT NUMBER

6. AUTHOR(S)
James F. Newill, Bernard J. Guidos, and Carl D. Livecchia

5d. PROJECT NUMBER
1L1622618.H80

5e. TASK NUMBER

5f. WORK UNIT NUMBER

7. PERFORMING ORGANIZATION NAME(S) AND ADDRESS(ES)
U.S. Army Research Laboratory
ATTN: AMSRL-WM-BC
Aberdeen Proving Ground, MD 21005-5066

8. PERFORMING ORGANIZATION REPORT NUMBER
ARL-TR-3039

9. SPONSORING/MONITORING AGENCY NAME(S) AND ADDRESS(ES)
OPM-MAS
ATTN: R. Darcy
Picatinny Arsenal, NJ 07806-5000

10. SPONSOR/MONITOR'S ACRONYM(S)

11. SPONSOR/MONITOR'S REPORT NUMBER(S)

12. DISTRIBUTION/AVAILABILITY STATEMENT
Approved for public release; distribution is unlimited.

13. SUPPLEMENTARY NOTES

14. ABSTRACT

This report compares a priori gun-projectile dynamic simulations to experimental ballistic jump test data for seven 120-mm prototype kinetic energy (KE) projectiles and describes the methodology used for the comparison. The projectiles contain significant differences in their charge, subprojectile, and sabot designs that span the design parameters encountered in KE cartridge development. In such tests, four or more sets of orthogonal radiograph images (x-rays), which are typically used to characterize the state of the projectile at muzzle exit, can be directly compared to predictions from ARL's gun-projectile dynamic simulation (GPDS) codes.
The results from these comparisons show that the GPDS codes were able to predict the ballistic experimental results except for the transverse center-of-gravity jump velocity in two cases. For the two cases, the difference in predicted and experiment is shown to occur when a high average rate is seen at the muzzle exit and is probably due to the timing error associated with muzzle exit.

15. SUBJECT TERMS
gun projectile dynamic simulations, kinetic energy projectile, jump testing

16. SECURITY CLASSIFICATION OF:			17. LIMITATION OF ABSTRACT	18. NUMBER OF PAGES	19a. NAME OF RESPONSIBLE PERSON
a. REPORT	b. ABSTRACT	c. THIS PAGE			James F. Newill
UNCLASSIFIED	UNCLASSIFIED	UNCLASSIFIED	UL	30	19b. TELEPHONE NUMBER *(Include area code)* 410-278-6097

Standard Form 298 (Rev. 8/98)
Prescribed by ANSI Std. Z39.18

Contents

List of Figures

List of Tables

Acknowledgments

A study of this magnitude requires a coordinated effort and the support of many people. The principal organizations are Project Manager Maneuvering Ammunition Systems program office, U.S. Tank-automotive and Armaments Command/Armament Research, Development, and Engineering Center, Alliant Techsystem Inc., and General Dynamics Ordnance and Tactical Systems. Their leadership, expertise, and experience are invaluable. This study relied heavily on supercomputers supplied by the Department of Defense's high performance computing initiative (specifically, those at the Major Shared Resource Center at the U.S. Army Research Laboratory).

INTENTIONALLY LEFT BLANK.

1. Introduction

Recently, emphasis has been placed on the direct-fire accuracy of tank main armament systems to enhance the lethality of this class of weapons and to improve accuracy of supersonic kinetic energy (KE) projectiles. A fundamental understanding of gun systems and projectile interaction is paramount to meeting this goal. The only direct means of studying the in-bore motion of the project and gun-projectile system interaction is through numerical simulation. To use the predicted results from these tools with confidence requires ballistics validation. The best approach for validation of the U.S. Army Research Laboratory's (ARL) gun-projectile dynamic simulation (GPDS) codes is comparison with projectile motion data obtained from ARL ballistic jump test experiments.

This report starts with the jump model, which is the basis for defining accuracy performance used in both GPDS and the jump experiments. Next, a description of how a jump test is conducted along with the instrumentation used in the test and the data is collected. This is followed by a brief description of the simulation technology along with how the data are reduced. These two efforts show how the data, which need to be compared, are obtained. To compare the data sets, a methodology is required. The methodology is presented along with seven examples.

2. Jump Model

The complete set of jump test data provides a range of information concerning the launch and flight behavior of the rounds. A substantial portion of the data is used to construct a jump diagram for each shot. The jump diagrams are based upon a jump closure model that characterizes the launch and flight aspects of the rounds, as well as providing a basis for statistical analysis of the entire set of rounds. The jump model has been presented along with the techniques in references (*1–6*) and is briefly reviewed here.

The total jump of a particular shot can be defined as the vector angle between projectile target impact and the pretrigger line of fire (LOF), with gravity drop removed. The jump vector is defined using the nomenclature introduced in Figure 1.

The boresight LOF is established as the line connecting the center of the muzzle and boresight point obtained by the muzzle borescope. The gravity drop can be extracted separately from various data sources, including the radar track, and is well understood. The LOF and gravity drop together establish a target aim point from which the target impact point is measured. The

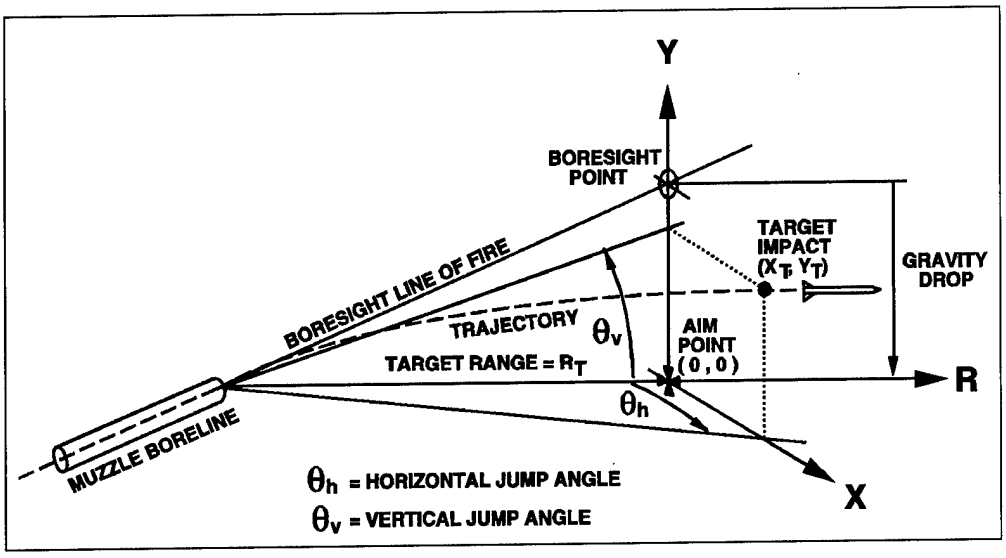

Figure 1. Illustration of jump angles.

resulting vector is denoted as (X_T, Y_T), with the subscript "T" representing the values at the target impact point. For the KE projectiles of interest here, the magnitude of this vector is small enough compared to the target range, R_T, such that the vector is converted directly into an angle, in radians, when divided by the range to form the total jump, $\overline{\theta}$, (small angle assumption), i.e.,

$$\overline{\theta} = \theta_h \hat{i} + \theta_v \hat{j} \cong {}^{X_T}\!/_{R_T}\, \hat{i} + {}^{Y_T}\!/_{R_T}\, \hat{j}. \quad (1)$$

In the previous expression, θ_h and θ_v are the horizontal and vertical components, respectively, of the total jump. The unit vector $\hat{i}$ is oriented to the gunner's right (positive X in Figure 1) and the unit vector $\hat{j}$ is oriented up (positive Y in Figure 1), and these orientations represent jump coordinates as used in this report.

The jump closure model, shown in Figure 2, follows that which has been presented in previous jump tests (*1*, *5*). The origin is defined as the intersection of the horizontal and vertical axes (labeled H and V) and represents the aim point. The aim point is determined by subtracting the gravity drop from the boresight LOF. The target impact point is denoted as a solid circle. A set of five vectors is defined whose summation is equal to the vector, whose tail is located at the aim point, and whose head is located at the target impact point. These vectors are jump component vectors, each having a horizontal and vertical component, and are defined as follows:

- Muzzle Pointing Angle (*PA*)—The muzzle pointing angle at the time of shot exit relative to the aim point.
- Muzzle Crossing Velocity Jump (*CV*)—The angular deviation corresponding to muzzle lateral motion, obtained by dividing the muzzle lateral velocity at shot exit by the projectile launch velocity.

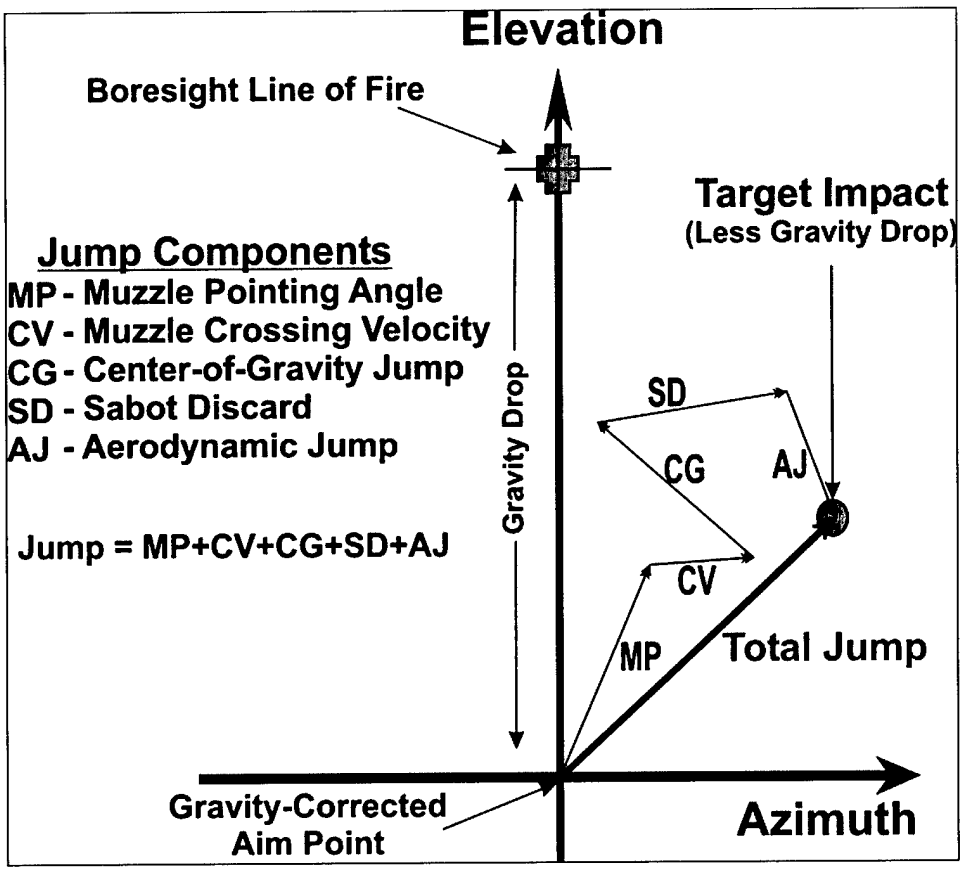

Figure 2. Jump closure model.

- Center-of-Gravity Jump (*CG*)—The angular deviation of the subprojectile center of gravity *CG* at the muzzle relative to the instantaneous bore centerline at shot exit. Also referred to in previous jump tests as the jump due to mechanical disengagement of the projectile from the gun tube. The vector arises from the center-of-gravity motion caused by the balloting interaction between the projectile and the gun tube.
- Sabot Discard Jump (*SD*)—The angular deviation of the projectile center of gravity attributable to the transverse disturbance arising from the sabot discard process.
- Aerodynamic Jump (*AJ*)—The angular deviation of the projectile's center of gravity attributable to aerodynamic lift forces associated with the free-flight projectile yawing motion. The source of the angular deviation is the angular rate at muzzle exit combined with the angular impulse caused by sabot discard.

In addition, the total *CG* (CG_{TOT}) is defined as the sum of the *PA*, *CV*, and *CG* vectors. The CG_{TOT} jump represents the angular deviation of the center of gravity at muzzle exit, relative to the pretrigger LOF. CG_{TOT} represents the transverse velocity of the projectile relative to the ground. This quantity is very convenient for making comparisons between jump testing and

simulation data because it is directly measured in the x-rays and directly computed from the GPDS codes.

3. Instrumentation and Test Apparatus

Figure 3 is an illustration of the primary instrumentation situated around the tank and the LOF. The measurement techniques follow the general set up and procedures described in reports of previous tests conducted at Aberdeen Proving Ground, MD (*1–3*, *5*, *6*). Table 1 lists the approximate ranges of the instrumentation.

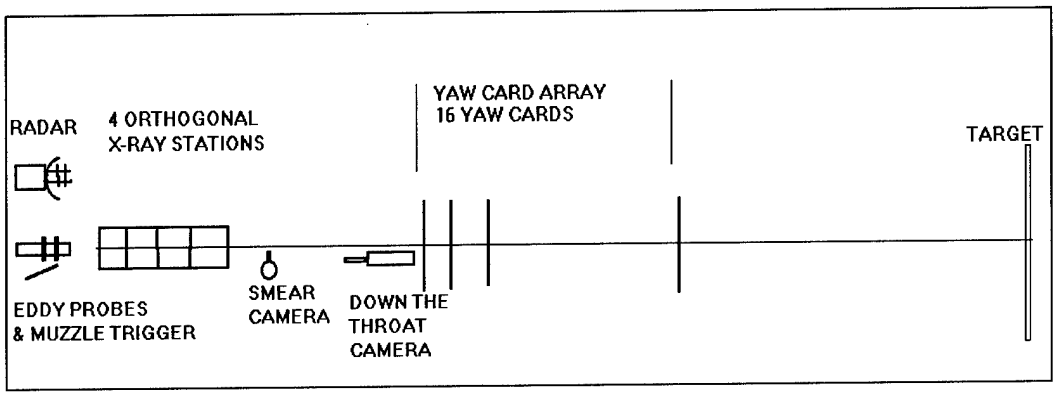

Figure 3. Instrumentation setup.

Table 1. Distances for instrumentation positions as measured from muzzle.

Instrumentation	Range
Eddy probe station no. 1	–0.495
Eddy probe station no. 2	–0.343
X-ray no. 1	0.5
X-ray no. 2	2.5
X-ray no. 3	4.5
X-ray no. 4	7.5
Orthogonal smear camera	10
High-speed video camera	30
Yaw card no. 1	37
Yaw cards no. 2–15	7-m spacing
Yaw card no. 16	142
Target	963

A muzzle pressure probe, used to provide an electronic trigger to the various recording devices, is positioned a few centimeters from the muzzle and supported by a cantilever that rotates away from the muzzle when impacted by the initial blast. Four sets of orthogonal x-ray stations are situated at four nonoverlapping axial stations within 10 m from the muzzle (Figure 4).

Figure 4. X-ray rig.

Each station consists of a pair of orthogonal 150-kV flash x-ray units and associated film with screen intensifiers enclosed and protected in wooden cartridge cases constructed prior to the test. The x-ray units are mounted onto a steel x-ray rig, shown in Figure 2, and the loaded cartridges secured onto the rig prior to each shot.

A set of eight proximity gauges (eddy probes) are mounted onto a specially constructed self-supporting aluminum rig slid over the gun tube to a location ~50 cm from the muzzle, as shown in Figure 5. The eddy probe rig is designed to secure two groups of four eddy probes each at two axial locations (~15 cm apart). Each eddy probe returns a voltage signal that corresponds to the distance between the probe tip and the gun. Prior to each shot, the eddy probes are adjusted within the rig to be positioned ~0.04 in from the tube surface, where a highly linear voltage signal exists. A temporary sunscreen, visible in Figure 4, is constructed from wood, cloth, and rope to shield the gun tube from direct sunlight and to minimize gun tube movement induced by disparate heating (*7*).

The complete set of eddy probe data is reduced in the posttest analysis into the form of *PA* and lateral displacement as a functions of time using the procedure reported by Bornstein and Haug (*1*). From these data, the *PA* and *CV* jump vector components can be obtained as part of the jump analysis. These data could be compared with data from the numerical simulations if the muzzle motion itself were simulated and stored during the numerical procedure. However, such is not the case for the numerical simulation approach used here, where projectile motion parameters, rather than muzzle motion parameters, are compared.

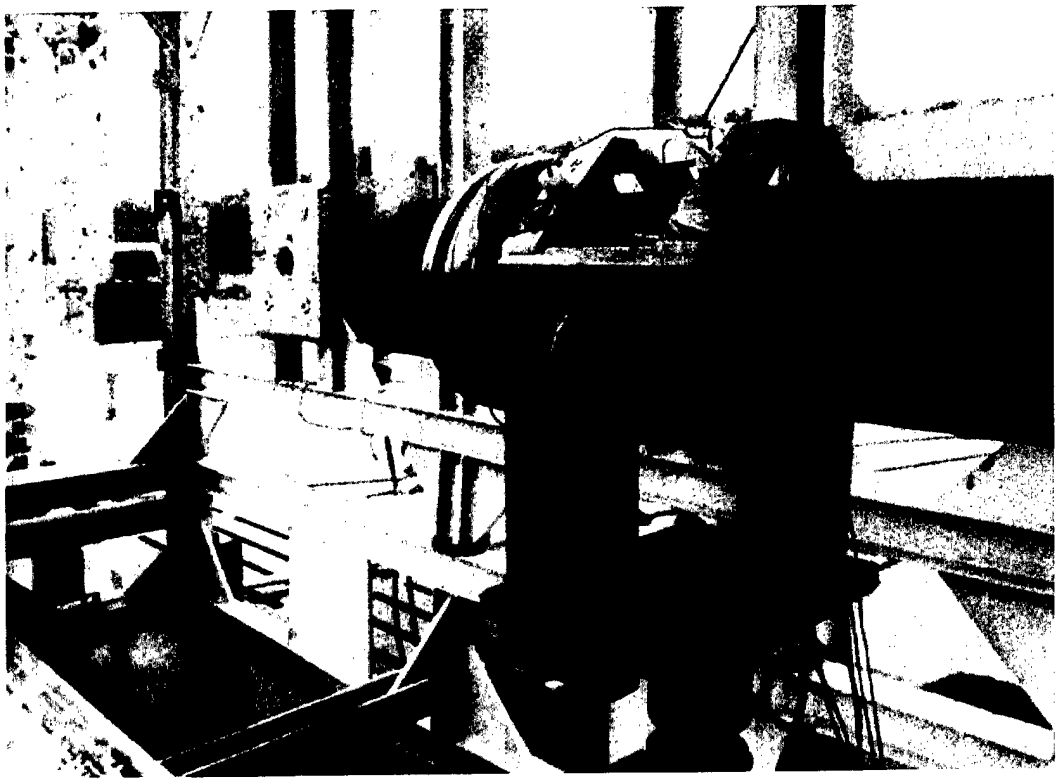

Figure 5. Eddy probe rig.

The jump test setup also consists of yaw card stations equally spaced along the LOF at axial locations between 37 and 142 m forward of the muzzle. The cloth target is located 963 m downrange of the muzzle. Two orthogonal color-smear camera images are collected at 10 m from the muzzle. The smear images are obtained by exposing highly sensitive film that is spooled at a high rate of speed as the projectile passes through the image domain. A "down-the-throat" high-speed video camera records each launch event using a line of sight acquired by a mirror positioned 30 m from the muzzle and ~0.6 m below the LOF. Weibel radar data are collected for each firing. With accompanying electronics and equipment, the instrumentation provides the data and visual records necessary to calculate the set of jump components sought for the particular shot.

The general test procedure for each shot is as follows: The muzzle is aimed at a predetermined point on the target using a collimated borescope. This boresight point, typically the lower right corner of the square formed by the intersection of the horizontal and vertical cross, is then surveyed. The cardboard yaw cards are mounted to the wooden support frames and marked with horizontal and vertical reference lines using the boresight. The loaded x-ray cassettes are secured into the rig. A fiducial cable (a steel cable containing two reference beads at each x-ray station) is hung along the LOF, as shown in Figure 6.

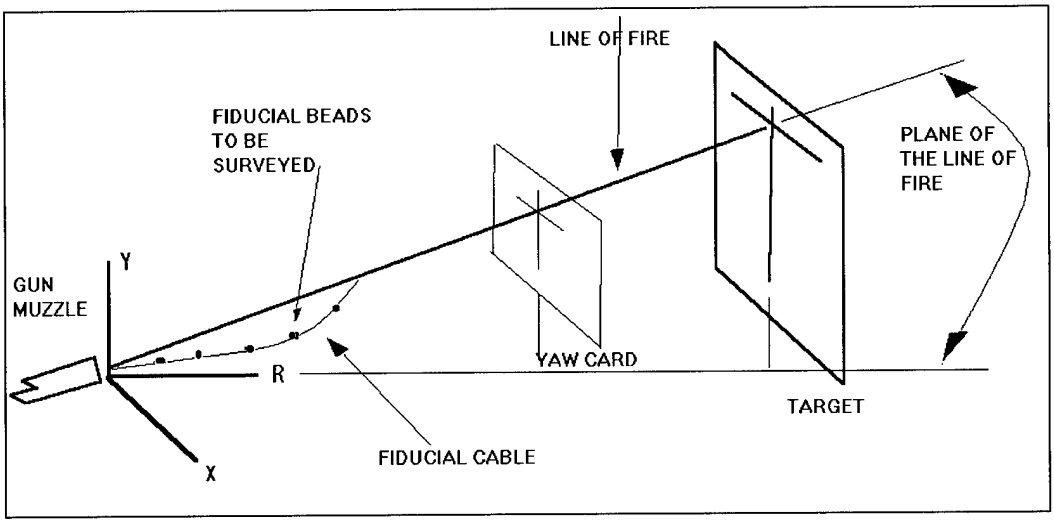

Figure 6. Test setup.

The steel fiducial cable is supported at the downrange end of the rig by a laterally adjustable pulley sighted to be near the LOF and at the breech by a metal plate. A mass of ~60 kg is hung from the downrange end of the cable, reducing the droop of the cable to a few millimeters. The applied mass forces the metal plate to abut tightly against the breech housing. The plate is laterally adjusted so that the cable is centered at the muzzle. The cable contains fiducial beads at each x-ray station to provide orientation and magnification references. A survey is conducted of the cable position at the muzzle, the pulley, and the fiducial beads. The x-ray film is exposed at a low power level to mark the bead locations, the cable is removed, and the pulley is lowered via a hinged platform attached to the x-ray rig. The eddy probes are adjusted, all instrumentation is set to initiate at pulse trigger, and firing commences.

4. Measured Projectile Muzzle Exit State and Jump Components

A single x-ray station is drawn schematically in Figure 7. After the fiducial cable and beads are exposed onto the x-ray film prior to the shot, the shot is fired and x-rays are taken of the projectile in flight. In each x-ray image, the position and orientation of the projectile are measured and can be related to the boresighted LOF determined from the cable image. Linear fits are made to the projectile lateral position and angular orientation, thus providing measured values of projectile angular and translational rates at muzzle exit. The projectile angular rate and projectile lateral translation rate at muzzle exit are the two quantities that are compared in the validation of numerical simulation with experimental measurement. The values are extracted from the data at a time that corresponds to shot exit, defined here as the instant in time when the rear bourrelet (also called the rear bore rider or bulkhead) mechanically disengages from the gun tube. At this time, the obturator undergoes a process of disintegration and the main blast uncorks.

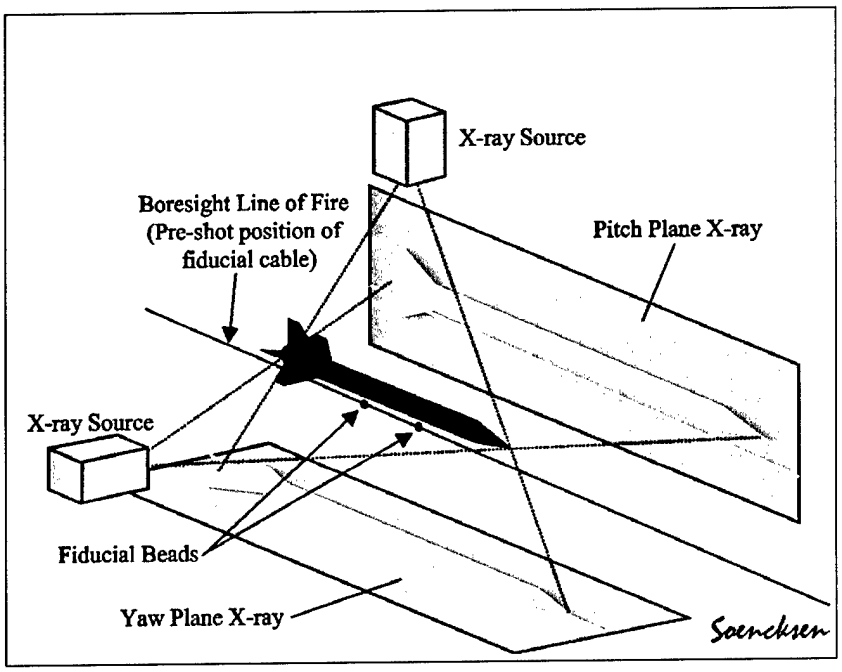

Figure 7. Orthogonal x-ray setup.

The CG_{TOT} jump vector is directly related to the lateral translation rate at muzzle exit. The CG_{TOT} jump is obtained by dividing the projectile lateral translation rate (a two-component vector, plane transverse to the LOF) by the projectile launch velocity. The AJ vector is closely related to the projectile angular rate at muzzle exit. Guidos and Cooper (*8*) used a linear impulse model to generalize the expression given by Murphy (*9*) that relates projectile angular rate at the muzzle and aerodynamic jump. For application to a KE projectile with sabot discard, the expression can be approximated and written in complex coordinates (the transformation between complex coordinates and range coordinates, consistent with that used by Guidos and Cooper [*8*] is not an issue of concern here) as

$$AJ = -k_t^2 \frac{C_{L\alpha}}{C_{M\alpha}} \left(\tilde{\xi}_0' + \tilde{\mathrm{J}}_l^* \right) , \tag{2}$$

where

k_t^2 = subprojectile nondimensional radius of gyration,

$C_{l.\alpha}$ = subprojectile aerodynamic lift force coefficient derivative,

$C_{M\alpha}$ = subprojectile aerodynamic pitching moment coefficient derivative,

$\tilde{\xi}_0'$ = subprojectile angular rate at muzzle exit (rad/caliber),

$\tilde{\mathrm{J}}_l^*$ = change in subprojectile angular rate attributable to sabot discard (rad/caliber),

$\tilde{\xi} = \alpha + i\beta$ = subprojectile angle of attack in complex coordinates,

α = pitch angle (positive up), and

β = yaw angle (positive nose left).

In equation 2, the subprojectile angular rate at muzzle exit, $\tilde{\xi}'_0$, is a measure of the total angular impulse applied to the projectile by the gun. The change in subprojectile angular rate attributable to sabot discard, $\tilde{J}_l^*$, is a measure of the total angular impulse applied to the subprojectile during the sabot discard process. Further discussion of the quantity $\tilde{J}_l^*$ is made by Guidos and Cooper (*8*).

To complete the discussion of jump components, it is noted that the *SD* jump vector is typically obtained through closure, where the aerodynamic jump vector is placed on the jump diagram so that its tip is coincident with the actual recorded projectile impact point. The *SD* jump vector is constructed that closure is achieved between the tip of the *CG* vector and the base of the *AJ* vector, as shown in Figure 2. As stated, this vector is actually a combination of the *SD* jump vector and the sum of all measurement errors, which are typically on the order of 0.2 mrad or less (*10*).

5. Numerical Simulation of Tank Gun Projectiles

GPDS codes use three-dimensional (3-D) finite element (FE) models of the M256 120-mm tank cannon launching projectiles. Figure 8 shows a typical model and the method is described in references (*11–32*). The hydrocode FE formulation was chosen to allow investigation of stress wave propagation due to elements of launch. The models are 3-D to capture the asymmetric response of the projectile and gun system resulting from the nonlinear path of the projectile during launch, asymmetric boundary conditions, general lack of symmetry in the centerline profiles of the gun tube, and asymmetric gun motion.

The projectiles and gun systems are both built in similar manners. Models are developed for the components and then integrated. Relative motion is obtained by defining the proper physics to allow interaction between the parts. One of the purposes of these types of studies is to estimate tank fleet performance. In order to do this, the projectile model is integrated into (and fired from) a number of gun models, each of which have unique tube centerlines. The propellant pressure loading for the gun system and projectile is generated from interior ballistic high velocity gun 2 (IBHVG2) (*33*), which provides good quality interior ballistic prediction for production charges.

The GPDS codes predict the transverse rates (velocity and angular rate) during the launch cycle (Figure 9). Three types of information are used from these predictions: the dynamic path,

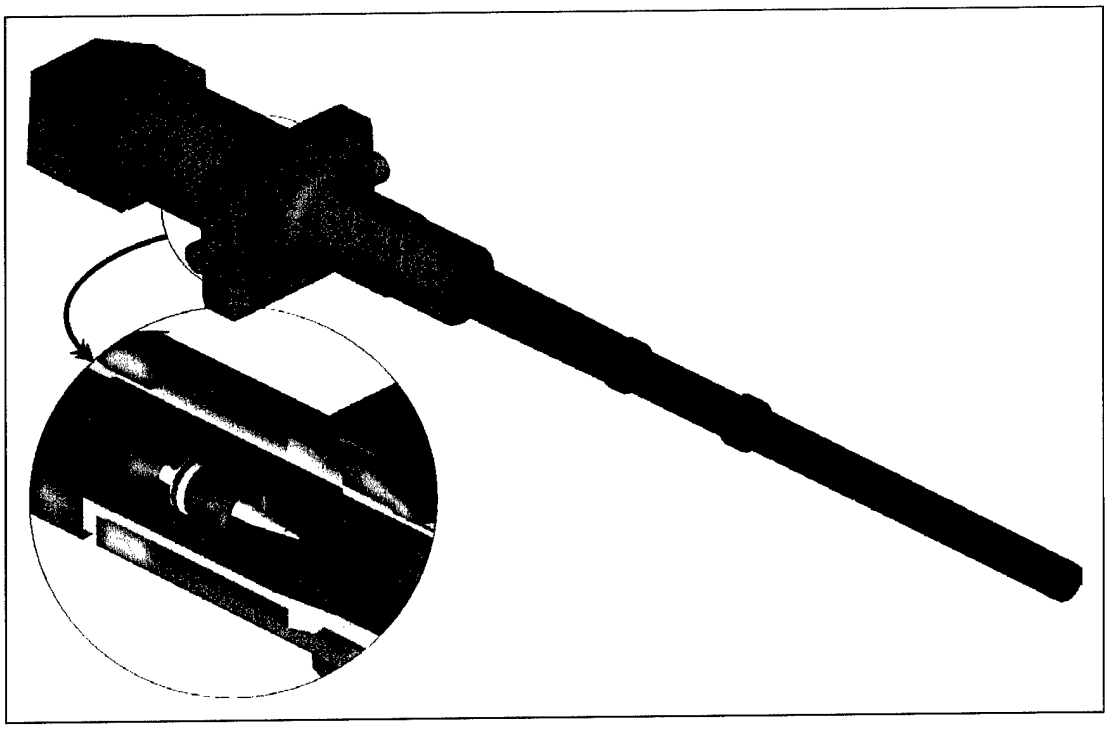

Figure 8. M1's M256 gun system with KE training projectile shown in bore.

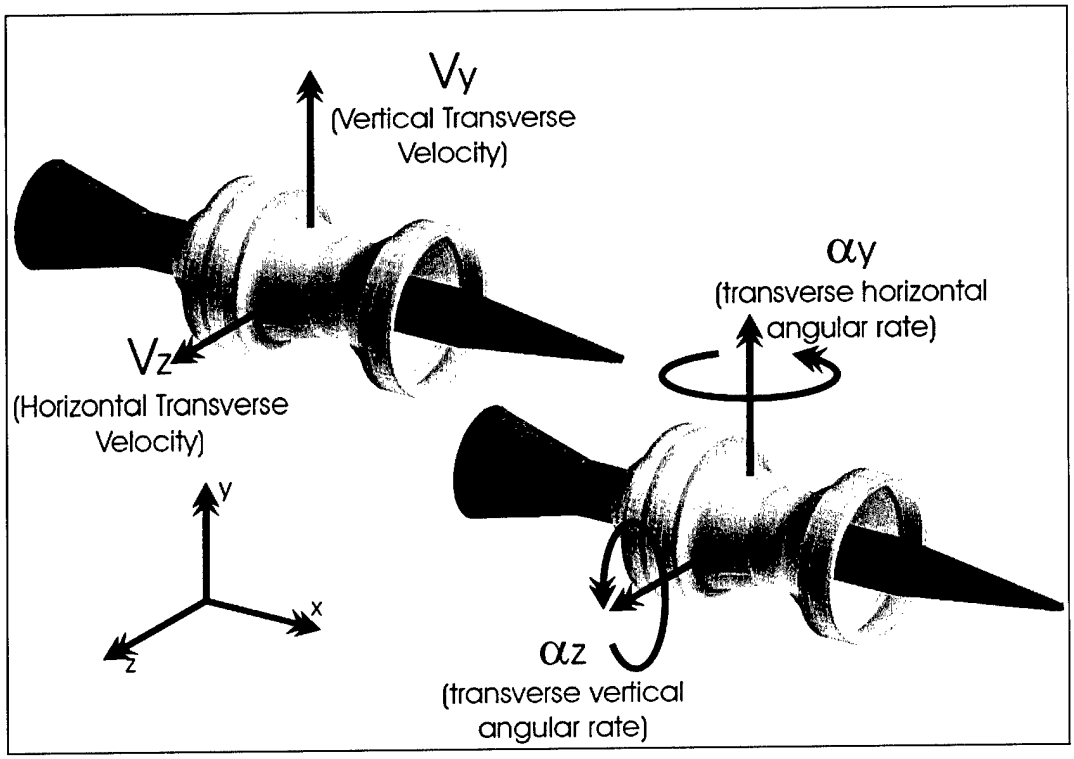

Figure 9. Definition of transverse rates.

variability in jump, and the average jump. The dynamic path gives qualitative information on the rate history of the projectile during the launch cycle. The variability and average jump predicted by the codes are related to accuracy errors where reduction in variability or error represents improved performance of the system.

To intentionally induce the variability into the dynamic path, which results in variability in the muzzle exit rates, a series of initial conditions are used. The initial condition that has the strongest influence is the initial cocking angle of the projectile in the forcing cone/bore. Because the diameter of the projectile's bourrelets is less than the interior bore and forcing cone diameter, there exists a clearance between the projectile and the gun tube. The angle between the longitudinal axis of the projectile and the axis of the chamber is defined as the cocking angle. Therefore, the cocking angle is relative to how the gun bore/forcing cone and chamber are manufactured, the projectile and cartridge's manufacturing dimensions, along with total run-out of the cartridge (how straight the cartridge is made).

There are an infinite number of ways that the projectile can be cocked in tube, but typically, the cocking angles used in simulations are up, down, left, right, and straight. The cocking angles are calculated on a model-by-model basis using the specific dimension of the particular projectile/gun geometry. The projectile oriented with a "straight" cocking angle has the forward and rear bourrelet centered relative to the initial location of the projectile in the gun.

6. Methodology for Comparison of Jump Test Data to GPDS Data

In order to validate the gun codes, some type of methodology is required in order to compare various projectiles performance. Because the phenomena being predicted are nonlinear and stochastic in nature and the initial conditions are not known precisely on a shot-by-shot basis, the GPDS codes are used to predict an envelope of performance. This is consistent with the experimental methodology. Typically, a series of projectile shots is simulated to predict both the center of impact and variability. Essentially, in the gun codes, to induce the variability, the initial conditions are varied; then, a series of simulations is accomplished (*32*). Using these simulations, the range of angular rates and range of transverse velocities are predicted.

On a smaller scale, this is consistent with how the gun codes are used to predict performance. To define projectile "tank fleet" performance the same type of data is predicted, but it is combined with multiple gun systems at a range of temperatures. When comparing to experimental data only, the gun tube centerline and propellant temperatures from the test are used. Figure 10 shows how the envelope predicted from the simulations and measured in the experiment are compared. In Figure 10, there are four items of interest: the experimental data, predictions from the simulation, the envelope (variability) of performance from the simulation, and a 95% confidence level for the experimental data. The comparison between the experiment and

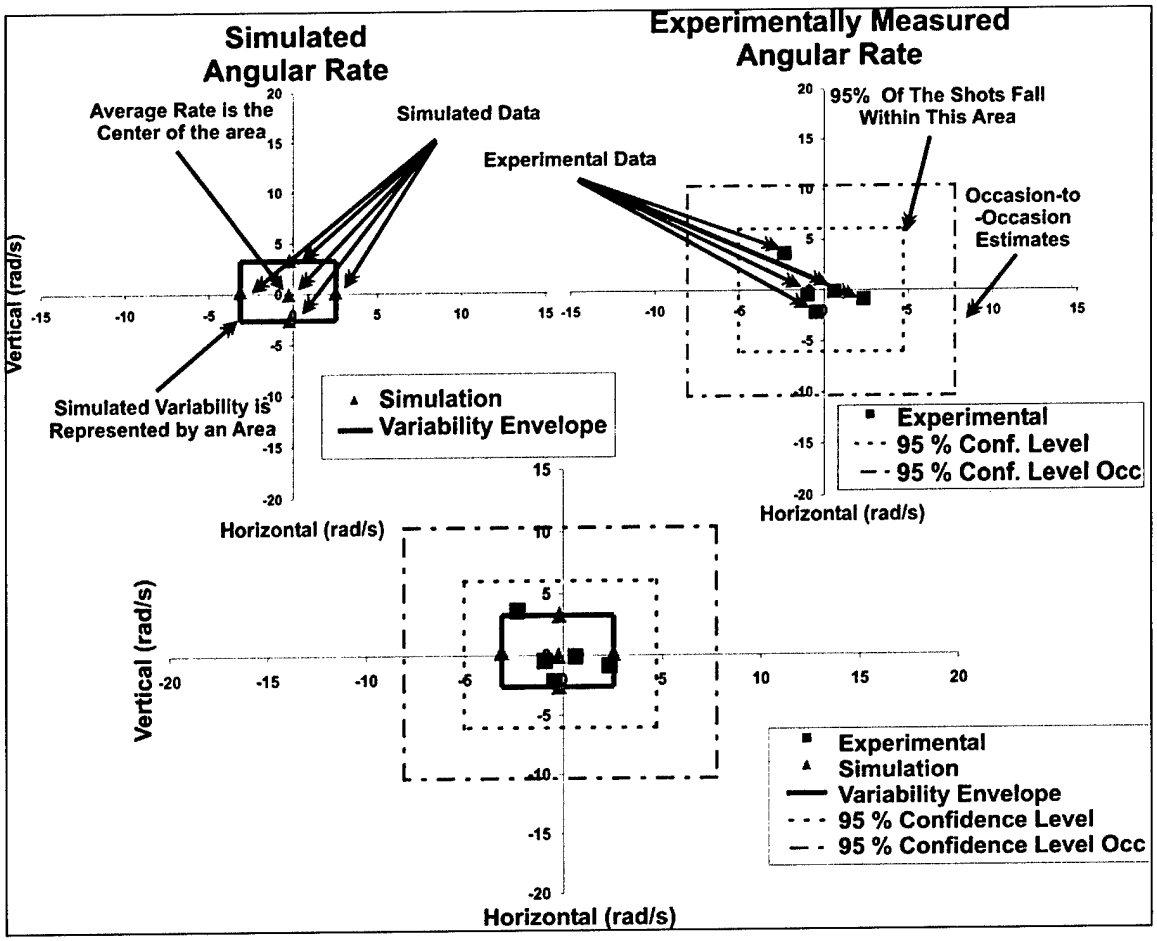

Figure 10. Simulation comparison with experimental results.

simulation is made through the relative sizes of the variability and the averages of predicted and measured data.

It is very important to note that the experiment is a ballistic phenomenon that is not entirely predictable. Even with production ammunition and with as many factors as possible controlled, there can be significant deviation of the shooting performance. For this reason, there can never be absolute comparison between the simulated data and the experimental data.

The variability predicted should typically be smaller than the variability (95% confidence level) in the experiment, although working with prototype projectiles complicates the situation. Prototype projectiles are made in small numbers with custom-designed propellant charges. Both the small numbers and the custom charge induce variability that would not be seen in a well-made production projectile. Other reasons for the variability in the experimental data to be larger than the simulation data are related to ambiguity in shot start (fracture of the case adapter), variability due to the propellant burning,* and the fracture problem at muzzle exit associated with

* The propellant can burn asymmetrically and generate large transverse pressure waves. Either effect can severely degrade the performance of the projectile or destroy it.

the breaking of the obturator. Each of these is significant and is attacked through other means as separate problems to reduce variability and improved projectile performance.

There are two ways that the average is compared to the experimental data. The first level compares the simulation data to the experimental data; the average should lie within the 95% confidence level of the experimentally measured values. Unfortunately, due to the nature of tank firing, a second envelope needs to be used. The issue is related to what is typically called occasion-to-occasion (occ-occ) error. It basically accounts for differences in the experimental data seen when firing from the same tank at two different times while still controlling the other factors of the experiment. The second box represents the uncertainty from this occ-occ error. The envelope is determined using empirical methods based on a history of shooting results. The average of the simulation data should lie within the occ-occ estimate for a good comparison.

7. Comparisons Between Experiment and Simulation

The predictions from the GPDS codes can be very useful if it can be related to the physical system. In this section, several examples are shown to depict the range of comparison between experiment and simulation. The ballistic data were obtained in jump tests conducted by ARL at the U.S. Army Aberdeen Test Center.

Seen in Figures 11–21, the experimental and simulated data compare well in both variability and average to the experimental data. In Figure 11, the simulation results are located somewhat lower than the actual experimental data, but are within the 95% confidence level of the experimental data, which show a good comparison. The variability of both the transverse velocity and the angular rate data is smaller than the experimental data as is expected, but the variability in the experimental results is high.

The comparison in Figure 12 is similar to Figure 11, the simulation data are within the 95% confidence level of the experimental data. Again, the variability in the simulation results is less than the experimental data. The variability in the experimental data is relatively large with the exception of the horizontal center of gravity rates.

Figure 13 shows a very good comparison between the experimental data and the simulation data. The average and variability data are very close to the actual experimental shots. There is still a lot of variability in the experimental horizontal center of gravity velocity.

Figure 14 shows similar quality of comparison as Figure 13. The average rates and variability in the rates compare very well. The experimental data show less variability than some of the results of the previous projectiles.

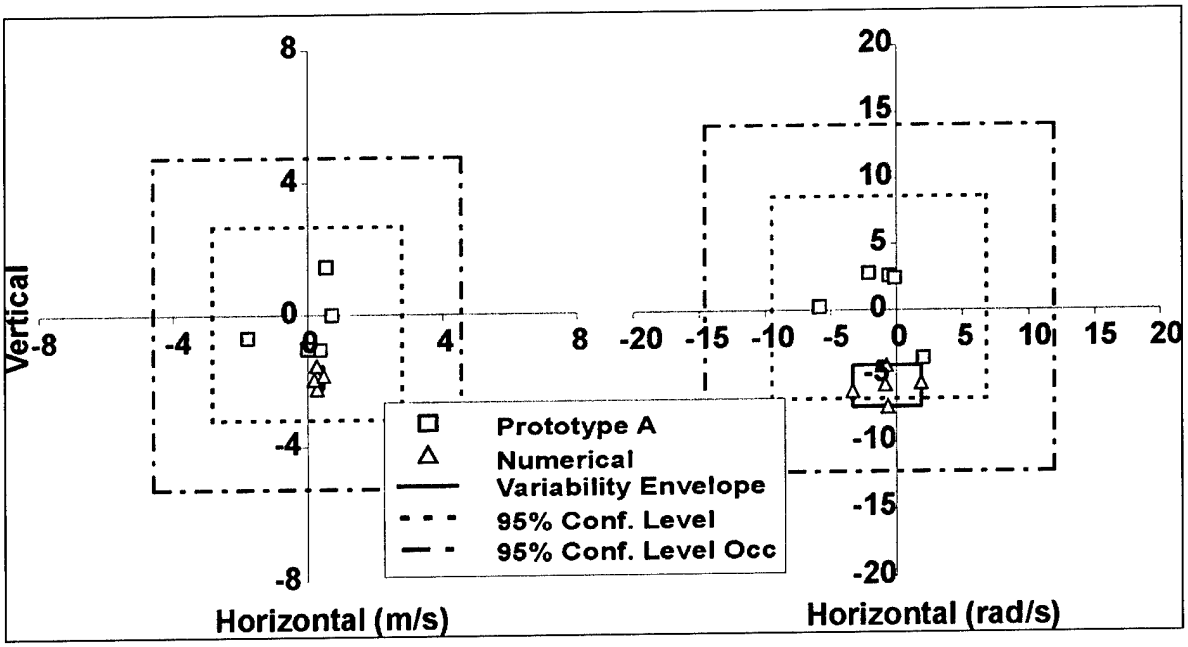

Figure 11. Transverse velocity and angular rate comparisons for projectile A.

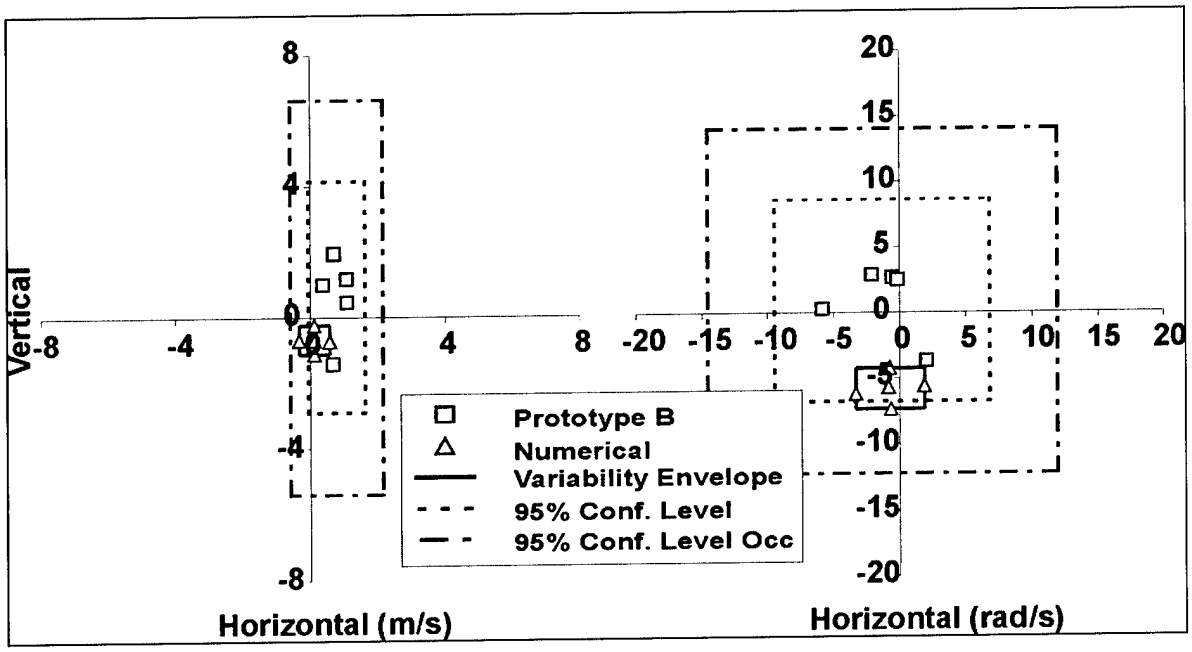

Figure 12. Transverse velocity and angular rate comparisons for projectile B.

Figure 15 also shows a good comparison, although the average of the center of gravity velocity is near the edge of the 95% confidence level. While the average is within the range of 95% confidence level corrected for occ-occ error, the result shows a trend that is more pronounced in the last two comparisons.

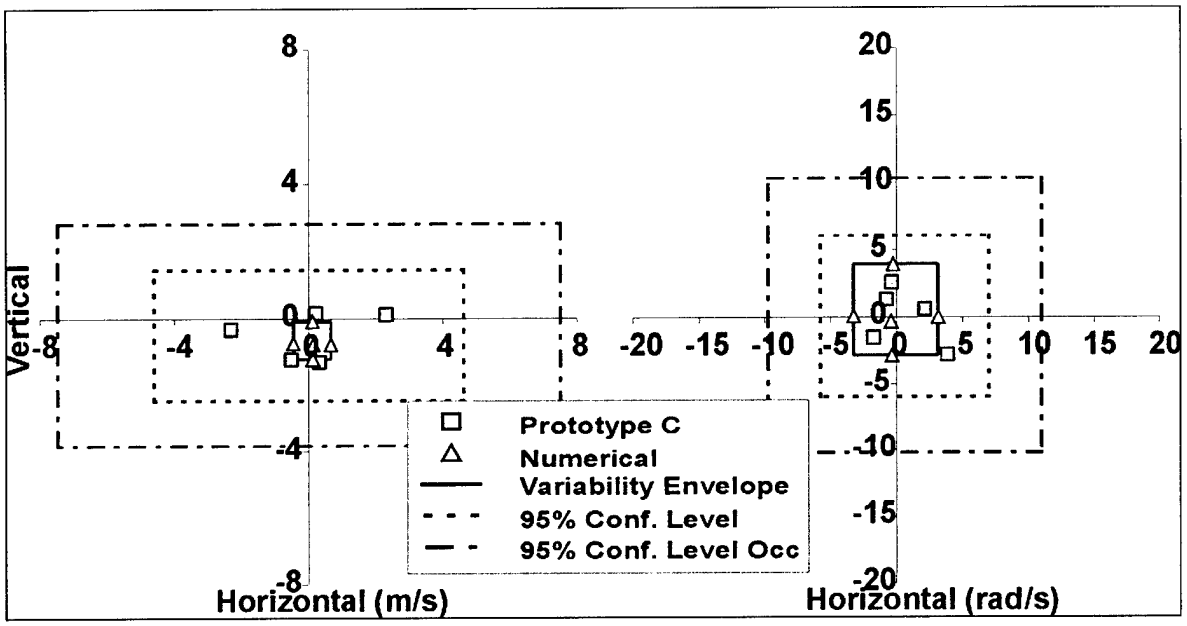

Figure 13. Transverse velocity and angular rate comparisons for projectile C.

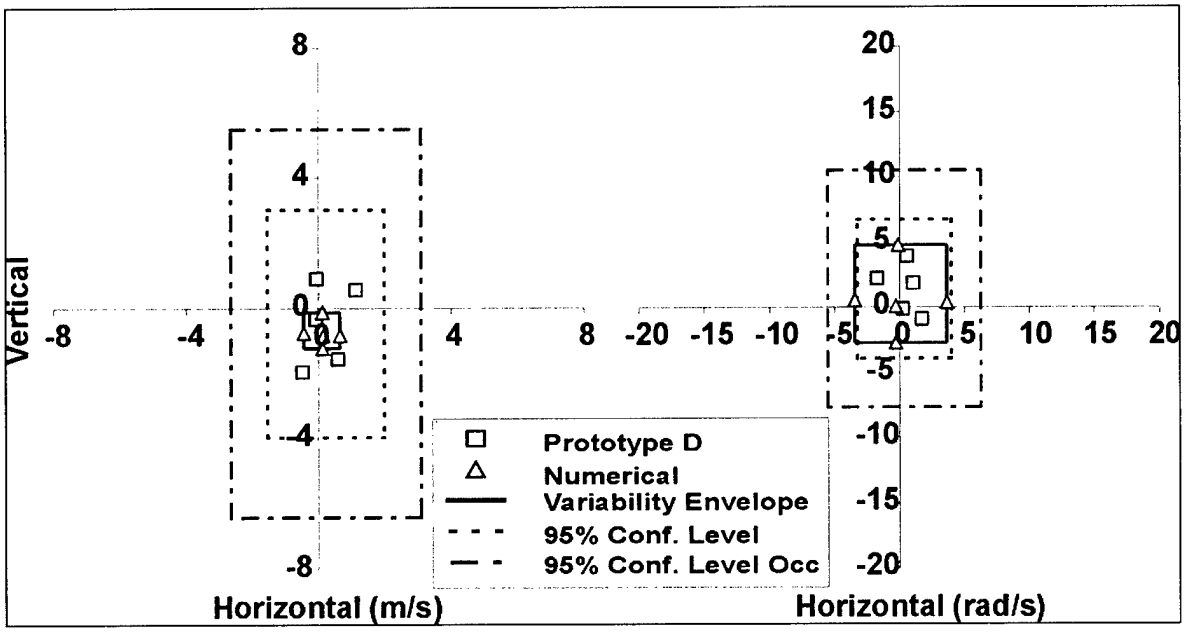

Figure 14. Transverse velocity and angular rate comparisons for projectile D.

Figures 16 and 17 show that the average of both the center of gravity velocity and the angular rates are offset from the experimental data. While the angular rate data are still within the 95% confidence level corrected for occ-occ error, the center of gravity velocity data are outside of the box. The variability data are reasonable for both of these projectiles, but the center of gravity velocity data are skewed in the vertical plane.

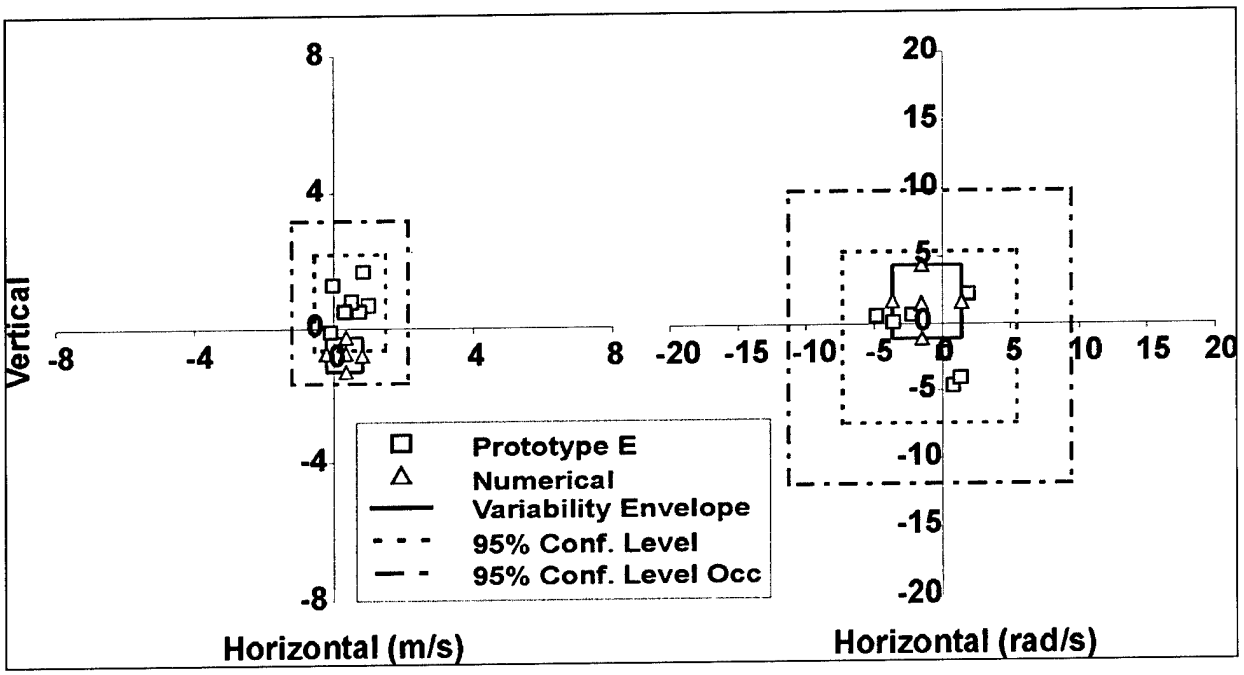

Figure 15. Transverse velocity and angular rate comparisons for projectile E.

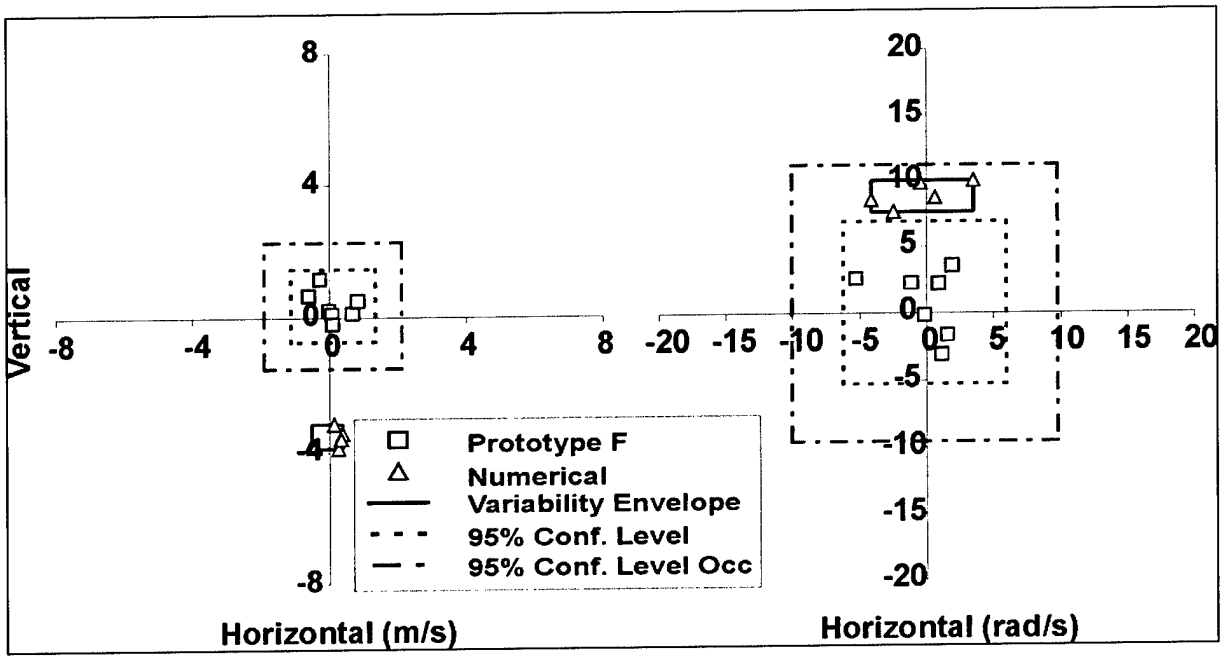

Figure 16. Transverse velocity and angular rate comparisons for projectile F.

Overall, the comparison is very good. Only in the last two figures are the average rates significantly different from the experiments, although the variability data are fine. In Figure 18, the rates of the horizontal velocity and horizontal angular rate can be seen to be changing rapidly near muzzle exit. The vertical component is seen to change much faster especially during the

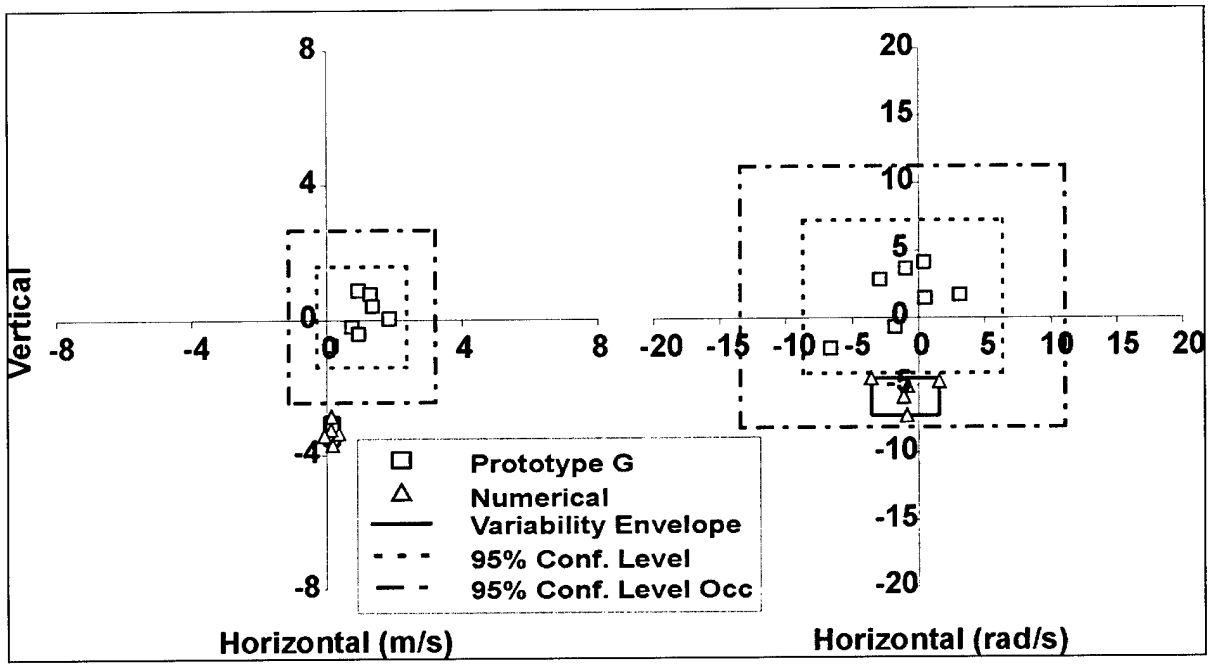

Figure 17. Transverse velocity and angular rate comparisons for projectile G.

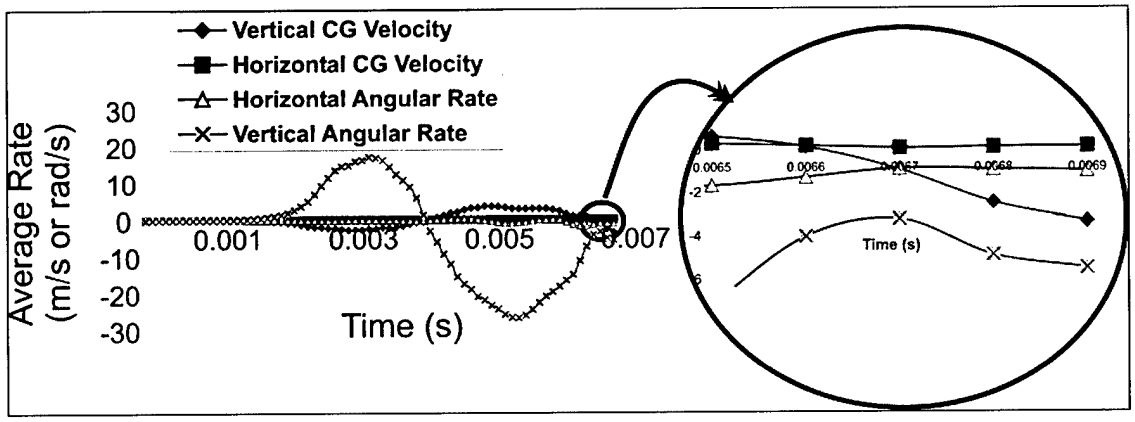

Figure 18. Average transverse rates and accelerations during launch for prototype G.

last 0.4 ms of travel. Also, if there is a time error in muzzle exit and the projectile actually exited earlier than predicted, then both horizontal components move toward zero, which is what was seen in the experiment. There are several aspects of the simulation that can cause variability in muzzle exit times relative to the experiment. The first is differences in muzzle exit time. While these differences are small in magnitude, they imply that the projectile exited early. Other problems with these predictions have to do with shot start and propellant variability. The shot

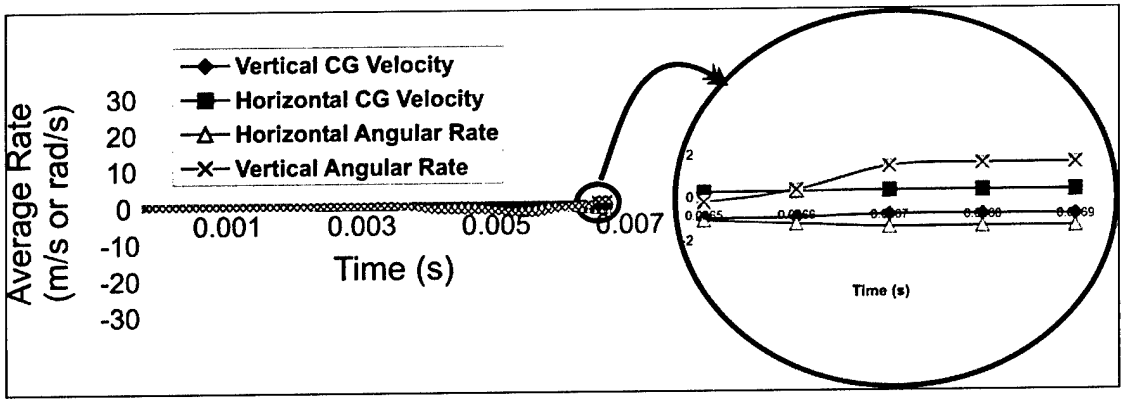

Figure 19. Average transverse rates and accelerations during launch for prototype E.

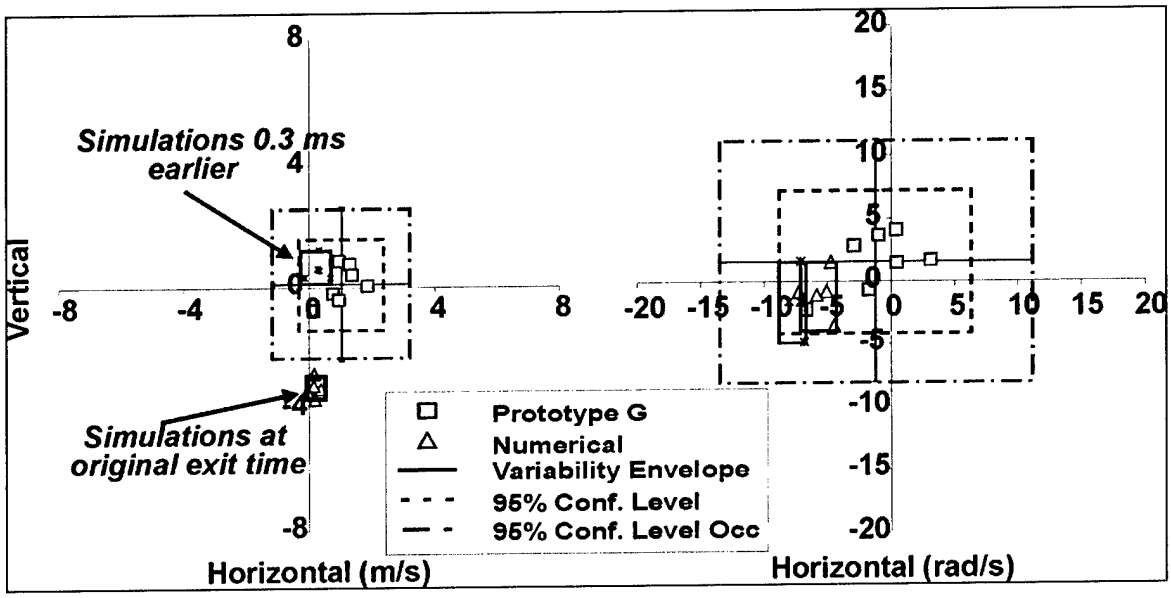

Figure 20. Multiple time comparisons for prototype G.

start has to do with the projectile not moving until the propellant has developed enough pressure to break the case-base adapter. The propellant issue deals with variability due to development of the flame and the symmetry of the burning. In any of these cases, the exit time can vary.

For the projectile design in Figure 19, examining the same quantities shows that the accelerations near muzzle are relatively low and that the change in rates is also very low. In each case, the simulation and experiment show a very good correlation and provide insight into how sensitive the performance is to small changes in muzzle exit time. Figures 20 and 21 show what happens to the experimental/simulation comparisons when these small time differences are considered. Figure 20 clearly shows that the transverse velocity matches well at the earlier time, whereas the angular rate data are not affected as much. Figure 21 shows the same type of comparison for a well-behaved projectile. Here, the comparisons are almost identical regardless of the exact exit time.

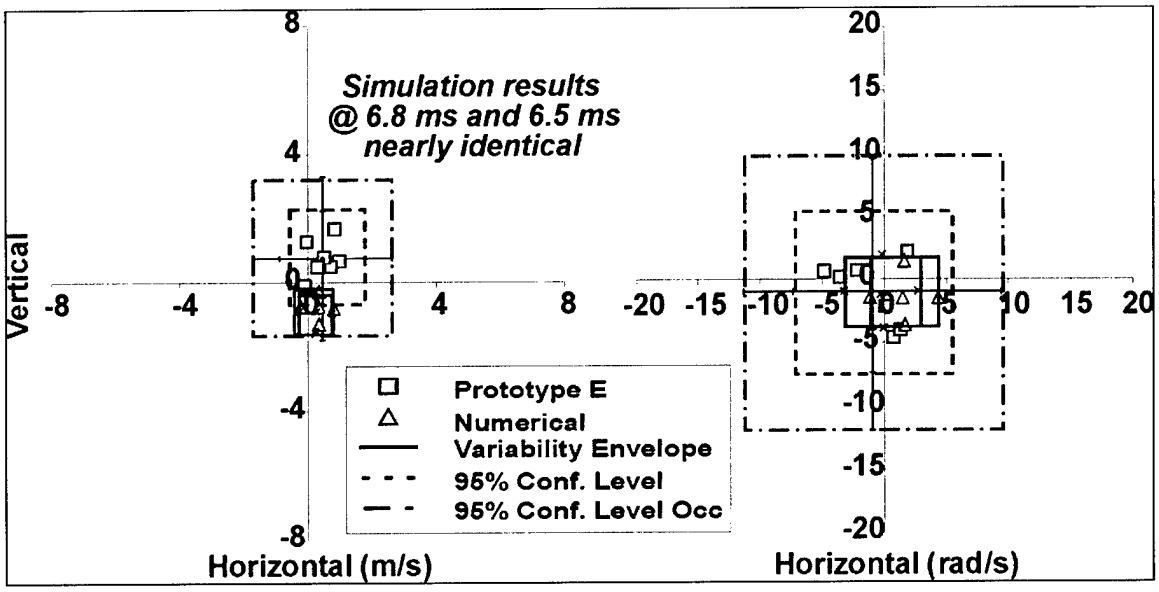

Figure 21. Multiple time comparisons for prototype E.

8. Conclusion

This report describes how to compare ballistic experimental data obtained from a precision jump test with a priori predictions made using ARL's GPDS codes. In addition to the methodology, seven examples were presented showing comparison between jump tests and GPDS codes for various types of prototype KE projectiles. The various KE projectiles have different types of sabots and rod configurations.

The results from these comparisons showed that the GPDS codes were able to predict the ballistic experimental results except for the transverse center of gravity velocity in two cases. For the two cases, the difference between simulation and experiments was shown to occur when high average rates were seen at muzzle exit and were probably due to timing errors associated with muzzle exit.

9. References

1. Bornstein, J.; Haug, B. *Gun Dynamics Measurements for Tank Gun Systems*; BRL-MR-3688; U.S. Army Ballistic Research Laboratory: Aberdeen Proving Ground, MD, May 1988.

2. Bornstein, J.; Celmins, I.; Plostins, P. *Launch Dynamics of Fin-Stabilized Projectiles*; AIAA Paper No. 89-3395; August 1989.

3. Bornstein, J.; Savick, D. S.; Lyon, D. H.; Schmidt, E. M.; Kietzman, J.; Deaver, D. Simulation of Tank Cannon Launch Dynamics. *Proceedings of The 7th U.S. Army Gun Dynamics Symposium*; May 1993.

4. Bornstein, J.; Celmins, I.; Plostins, P.; Schmidt, E. M. *Techniques for the Measurement of Tank Cannon Jump*; BRL-MR-3715; U.S. Army Ballistic Research Laboratory: Aberdeen Proving Ground, MD, December 1988.

5. Plostins, P.; Celmins, I.; Bornstein, J. *The Effect of Sabot Front Borerider Stiffness on the Launch Dynamics of Fin-Stabilized Kinetic Energy Ammunition*; AIAA Paper No. 90-0066; January 1990.

6. Schmidt, E. M.; Plostins, P.; Bundy, M. L. Flash Radiographic Diagnostics of Projectile Launch from Cannon; *Proceedings of 84th Flash Radiography Symposium*; E. A. Webster, Jr. and A. M. Kennedy, Eds., The American Society for Nondestructive Testing, 1984.

7. Bundy, M. L.; Gerber, N.; Bradley, J. W. *Thermal Distortion Due to Wall Thickness Variation and Uneven Cooling in an M256 120-mm Gun Barrel*; U.S. Army Research Laboratory: Aberdeen Proving Ground, MD, September 1993.

8. Guidos, B. J.; Cooper, G. R. *The Effect of a Simple Lateral Impulse on Kinetic Energy Projectile in Flight*; ARL-TR-2076; U.S. Army Research Laboratory: Aberdeen Proving Ground, MD, December 1999.

9. Murphy, C. H. *Free Flight Motion of Symmetric Missiles*; BRL-TR-1216; U.S. Army Ballistic Research Laboratories: Aberdeen Proving Ground, MD, July 1963.

10. Lyon, D. H.; Savick, S.; Schmidt, E. M. *Computed and Measured Jump of 120mm Cannon*; AIAA Paper No. 91-2898; July 1991.

11. Rabern, D. A. *Axially Accelerated Saboted Rods Subjected to Lateral Forces*; ARL-CR-671; U.S. Army Ballistic Research Laboratory: Aberdeen Proving Ground, MD, August 1991.

12. Rabern, D. A. *Axially Accelerated Saboted Rods Subjected to Lateral Forces*; LA-11494-MS; Los Alamos National Laboratory: Los Alamos, NM, March 1989.

13. Wilkerson, S. A.; Hopkins, D. *Analysis of a Balanced Breech System for the M1A1 Main Gun System Using Finite Element Techniques*; ARL-TR-608; U.S. Army Research Laboratory: Aberdeen Proving Ground, MD, November 1994.

14. Burns, B. P.; Newill, J. F.; Wilkerson, S. A. In-Bore Projectile Gun Dynamics; *Proceedings of the 17th International Ballistics Symposium*; Midran, South Africa, 26 March 1998.

15. Newill, J. F.; Burns, B. P.; Wilkerson, S. A. *Overview of Gun Dynamics Numerical Simulations*; ARL-TR-1760; U.S. Army Research Laboratory: Aberdeen Proving Ground, MD, July 1998.

16. Newill, J. F.; Hoppel, C. P. R.; Drysdale, W. H. *Comparison of Launch Mechanics and Dynamics From the M1A1 M256 Gun System for the M829A2 Kinetic Energy Long Rod Fin Stabilized Projectile Containing Different Penetrator Materials*; ARL-TR-1671; U.S. Army Research Laboratory: Aberdeen Proving Ground, MD, April 1998.

17. Newill, J. F.; Wilkerson, S. A.; Hoppel, C. P. R.; Drysdale, W. H. Numerical Simulation of Launch Interaction of Kinetic Energy Long Rod Fin-Stabilized Projectiles and M1A1 Abrams M256 Gun System With Comparison to Experimental Results; *Classified Ballistics Symposium*; Eglin AFB, FL, 11–14 May 1998.

18. Newill, J. F.; Guidos, B. J.; Livecchia, C. D. Comparison Between the M256 120-mm Tank Cannon Jump Test Experiments and ARL's Gun Dynamics Simulation Codes for Prototype KE; *10th U.S. Army Gun Dynamics Symposium*; Austin, TX, 23–25 April 2001.

19. Newill, J. F.; Hoppel, C. P. R.; Kamdar, D.; Guidos, B. J.; Drysdale, B.; Livecchia, C.; Luciano, M. *Geometric and Material Changes to the Forward Bourrelet to Optimize Performance of KE Ammunition*; ARL-TR-2328; U.S. Army Research Laboratory: Aberdeen Proving Ground, MD, September 2000.

20. Newill, J. F.; Hoppel, C. P. R.; Kamdar, D. S.; Guidos, B. J.; Drysdale, W. H. Geometric and Material Changes to the Forward Bourrelet to Optimize Performance of Kinetic Energy Ammunition; *Proceedings of the 3rd Joint Classified Ballistics Symposium*; San Diego, CA, 1–4 May 2000.

21. Newill, J. F.; Hoppel, C. P. R.; Soencksen, K. P.; Plostins, P. Simulation of the M865 Kinetic Energy Projectile With Experimental Validation; *Proceedings of the 18th International Ballistics Symposium*; San Antonio, TX, November 1999.

22. Newill, J. F.; Hoppel, C. P. R.; Drysdale, W. H.; Kamdar, D. S. *Effects of Bourrelet Stiffness on the Interior Ballistic Performance of Kinetic Energy Ammunition*; ARL-TR-2002; U.S. Army Research Laboratory: Aberdeen Proving Ground, MD, June 1999.

23. Newill, J. F.; Hoppel, C. P. R.; Drysdale, W. H.; Kamdar, D. S. Effects of Bourrelet Stiffness on the Interior Ballistic Performance of Kinetic Energy Ammunition; *1999 Joint Classified Ballistics Symposium Conference Proceedings*; Monterey, CA, 3–6 May 1999.

24. Newill, J. F.; Garner, J.; Soencksen, K. P.; Hoppel, C. P. R. Launch Dynamics of the 120-mm M831A1 Heat Training Projectile; *10th U.S. Army Gun Dynamics Symposium*; Austin, TX, 23–25 April 2001.

25. Newill, J. F.; Wilkerson, S. A.; Hoppel, C. P. R.; Drysdale, W. H. Numerical Simulation of Composite Kinetic Energy Projectiles Launched by an M1A1 Abrams M256 Gun System; *Proceedings of the 30th SAMPE Technical Conference*; San Antonio, TX, 23 October 1998.

26. Newill, J. F.; Wilkerson, S. A.; Hoppel, C. P. R.; Drysdale, W. H. Numerical Simulation of Launch Interaction of Kinetic Energy Long Rod Fin-Stabilized Projectiles and M1A1 Abrams M256 Gun System with Comparison to Experimental Results; *Classified Ballistics Symposium Proceedings*; Eglin AFB, FL, 11–14 May 1998.

27. Newill, J. F.; Hoppel, C. P. R.; Drysdale, W. H. *Comparison of Launch Mechanics and Dynamics from the M1A1 M256 Gun System for the M829A2 Kinetic Energy Long Rod Fin Stabilized Projectile Containing Different Penetrator Materials*; ARL-TR-1671; U.S. Army Research Laboratory: Aberdeen Proving Ground, MD, April 1998.

28. Soencksen, K. P.; Newill, J. F.; Garner, J. M.; Plostins, P. Comparison of the 120-mm M831A1 Projectile's Experimental Launch Dynamic Data With Hydrocode Gun-Projectile Dynamic Simulations; *10th U.S. Army Gun Dynamics Symposium*; Austin, TX, 23–25 April 2001.

29. Bundy, M. L.; Newill, J. F.; Hoppel, C. P. R. *A Notional Redesign of the M865E3 Obturator*; ARL-TR-2325; U.S. Army Research Laboratory: Aberdeen Proving Ground, MD, September 2000.

30. Bundy, M. L.; Newill, J. F.; Hoppel, C P. R. A Notional Redesign of the M865E3 Obturator; *Proceedings of the 3rd Joint Classified Ballistics Symposium*; San Diego, CA, 1–4 May 2000.

31. Guidos, G.; Plostins, P.; Webb, D.; Newill, J. F. *120-mm Tank Gun Accuracy Demonstrator (TGAD) Jump Test*; ARL-TR-2199; U.S. Army Research Laboratory: Aberdeen Proving Ground, MD, December 1999.

32. Wilkerson, S. *The Effect of Initial and Gun Mount Conditions on the Accuracy of Kinetic Energy (KE) Projectiles*; ARL-TR-895; U.S. Army Research Laboratory: Aberdeen Proving Ground, MD, November 1995.

33. Anderson, R. D.; Fickie, K. D. *IBHVG2 - A User's Guide*; BRL-TR-2829, U.S. Army Ballistic Research Laboratory: Aberdeen Proving Ground, MD, 1987.